

# Internal Ballistics of a Boron Containing Solid Fuel Ramjet

Hertzel Kadosh\* and Benveniste Natan\*\*

Faculty of Aerospace Engineering, Technion – Israel Institute of Technology, Haifa, Israel

\* Graduate Student

khertzel@campus.technion.ac.il.

\*\* Professor, Head, Fine Rocket Propulsion Center

aerben@technion.ac.il

## Abstract

This study focuses on parametric investigation of the internal ballistics of a Boron containing solid fuel ramjet. A 2-D axisymmetric model of ramjet combustor, at Mach 2.5 was solved numerically utilizing the ANSYS FLUENT CFD code. Simulations were made for different parameters and were compared to theoretical performance. The solid fuel regression rate depends on the port diameter and it decreases with time. Thrust regulation of ramjet engine was demonstrated using bypass air. The specific impulse decreases with boron content probably because of low combustion efficiency at low pressure.

## Nomenclature

### Variables

$A$	= reaction constant
$B$	= Spalding number
$BR$	= bypass ratio
$C_D$	= drag coefficient
$C_p$	= specific heat
$d$	= diameter
$D$	= diffusion coefficient
$E$	= energy
$E_a$	= activation energy
$f_M$	= mass fraction
$h$	= enthalpy
$J$	= mass flux
$k$	= thermal conductivity
$M$	= molar mass
$Nu$	= Nusselt number
$p$	= pressure
$R_B$	= molar rate of boron consumption
$R_E$	= molar evaporation rate of boric oxide
$R_H$	= molar rate of oxide removal by water
$R, R_u$	= universal gas constant
$Re$	= Reynolds number
$S_m$	= mass source
$S_h$	= enthalpy source due chemical reaction
$Sc$	= Schmidt number
$T$	= temperature
$u$	= axial velocity
$v$	= radial velocity
$X_i$	= molar fraction of species $i$
$Y_i$	= mass fraction of species $i$

### Greek

$\delta$	= boron oxide layer thickness
$\mu$	= viscosity
$\rho$	= density

### Subscripts

$l$	= laminar
$p$	= particle
$s$	= surface
$t$	= turbulent

## 1. Introduction

The Ramjet engine is a simple air-breathing device without any moving parts such as compressor and turbine. The basic idea behind ramjet propulsion is aerodynamic compression of air, making it suitable for supersonic flight speed. At Mach numbers of 2-4, the ramjet is highly efficient and has superiority over other types of engines.

The solid fuel ramjet (SFRJ) is the simplest type of a ramjet engine and it is characterized by increased energy density, simplicity (there is no need for fuel control, fuel storage and feeding system), relatively low cost and safety. The solid fuel combustor is made of a hollow cylinder of fuel, where air flows through its port and combustion takes place between the gasifying fuel surface and the bulk airflow. A diffusive flame is established within the boundary layer over the solid fuel surface.

Metal additives to the commonly used hydrocarbon fuels can provide better energetic performance, especially for volume-limited systems and Boron exhibits remarkable theoretical energetic performance (40% more than hydrocarbons) with the highest energy density of all elements, about three times of hydrocarbon fuels.

In order to realize these advantages, the boron particles must ignite and combust completely within a limited time residence. Since boron particles are initially coated with an oxide layer, which inhibits combustion and since boron has high boiling point (3930 K) this can become difficult [1].

Numerous studies and considerable effort were expended to define the mechanisms of boron particle ignition and combustion [2-7]. Macek observed in his studies that boron burning occurs in two stages. Following heat-up to about 1800-2000 K, the boron particle becomes luminous, glows for short period of time, fades out, and finally, provided the ambient temperature is sufficiently high, blossoms into a second stage of burning, which is much brighter and longer than the first stage [8].

King [1] has developed a model describing this observation. At the first stage, there is a heat-up from hotter surroundings and at sufficiently high particle temperature there is a self-heating by exothermic oxidation. Since the particle is initially coated with an oxide layer, the oxygen required for this reaction must diffuse through the surface liquid oxide. As the oxidation of the boron particle continues, it causes the oxide layer to thicken but at the same time the boron oxide evaporates from the particle surface and diffuses away at a rate which depends upon the particle temperature. Evaporation is an endothermic process that tends to cool and lower the rate of heating the particle, but given the right balance, the oxide layer will become thin and the particle temperature will continue to rise. The particle will rapidly eject its remaining oxide (causing the aforementioned dark period), and full-fledged combustion will occur. The modeled processes are shown in figure 1. Furthermore, Natan and Gany [9] showed that realization of the full energy potential of boron lies in the condensation of boron oxide, thus an afterburner with bypass air is required.

The present study focuses on modeling both the combustion of Hydroxyl-Terminated Poly-Butadiene (HTPB) as the solid fuel and the combustion of boron particle based on King's model, then the sensitivity of the SFRJ flow field and performance for several parameters was studied.

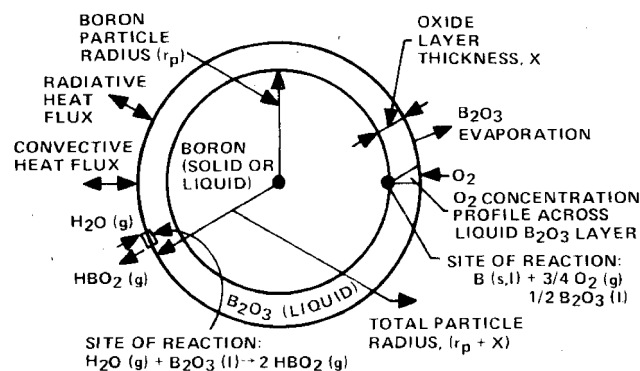


Figure 1: Boron particle ignition model processes [1].

## 2. Problem description

A 10 cm diameter, 0.5-0.75 m length solid fuel, 1 m length combustor with after-burner and converging-diverging nozzle (shown in figure 2) at Mach number 2.5 was modeled and numerically solved with ANSYS FLUENT CFD code. The computational model assumes steady state, 2-D axisymmetric, turbulent and reactive flow. The boundary conditions were obtained from 1-D flow model assuming an adapted to ambient pressure nozzle.

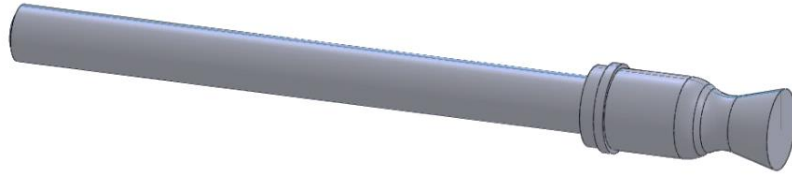


Figure 2: Control volume of the combustor.

Butadiene ( $C_4H_6$ ) is treated as the main product of HTPB pyrolysis [10] and boron particles are introduced from injections on the solid fuel surface. User defined functions (UDF) were written to describe the model of HTPB surface pyrolysis and to solve the solid-gas interface and to describe the model of boron ignition, combustion and oxide condensation.

### 3. Numerical model

Based on the above assumptions, the flow inside the combustor can be described by the Navier-Stokes governing equations of continuity, momentum, energy and species.

#### 3.1 Governing equations

Continuity

$$\frac{\partial}{\partial x}(\rho u) + \frac{\partial}{\partial r}(\rho v) + \frac{\rho v}{r} = S_m \quad (1)$$

Momentum (axial and radial)

$$\frac{1}{r} \frac{\partial}{\partial x}(r \rho u u) + \frac{1}{r} \frac{\partial}{\partial r}(r \rho v u) = -\frac{\partial p}{\partial x} + \frac{1}{r} \frac{\partial}{\partial x} \left[ r \mu \left( 2 \frac{\partial u}{\partial x} - \frac{2}{3} (\nabla \cdot \vec{V}) \right) \right] + \frac{1}{r} \frac{\partial}{\partial r} \left[ r \mu \left( \frac{\partial u}{\partial r} + \frac{\partial v}{\partial x} \right) \right] + F_x \quad (2)$$

$$\frac{1}{r} \frac{\partial}{\partial x}(r \rho u v) + \frac{1}{r} \frac{\partial}{\partial r}(r \rho v v) = -\frac{\partial p}{\partial r} + \frac{1}{r} \frac{\partial}{\partial x} \left[ r \mu \left( \frac{\partial v}{\partial x} + \frac{\partial u}{\partial r} \right) \right] + \frac{1}{r} \frac{\partial}{\partial r} \left[ r \mu \left( 2 \frac{\partial v}{\partial r} - \frac{2}{3} (\nabla \cdot \vec{V}) \right) \right] - 2 \mu \frac{v}{r^2} + \frac{2}{3} \frac{\mu}{r} (\nabla \cdot \vec{V}) + F_r \quad (3)$$

Where viscosity is given by the sum of laminar viscosity and turbulent viscosity:

$$\mu = \mu_l + \mu_t \quad (4)$$

Energy

$$\nabla \cdot (\vec{V}(\rho E + p)) = \nabla \cdot \left( k \nabla T - \sum_i h_i \vec{J}_i \right) + S_h \quad (5)$$

Where enthalpy is given by:

$$h = \sum_i Y_i h_i \quad (6)$$

$$h_i = \int_{T_{ref}}^T C_{p,i} dT \quad (7)$$

$$S_h = -\sum_i \frac{h_i^0}{M_i} R_i \quad (8)$$

$$p = \rho \frac{R}{M} T = \sum_i \frac{Y_i}{M_i} \rho RT \quad (9)$$

Species

$$\frac{\partial \rho u Y_i}{\partial x} + \frac{\partial \rho v Y_i}{\partial r} + \frac{\rho v Y_i}{r} = -\left[ \frac{\partial J_{ix}}{\partial x} + \frac{1}{r} \frac{\partial}{\partial r} (r J_{ir}) \right] + R_i + S_i \quad (10)$$

Where mass flux of species due to concentration gradient is given by:

$$\bar{J}_i = -\left( \rho D_{i,m} + \frac{\mu_i}{Sc_i} \right) \nabla Y_i \quad (11)$$

And turbulent Schmidt number is given by:

$$Sc_i = \frac{\mu_t}{\rho D_i} \quad (12)$$

Where the laminar viscosity is calculated according to kinetic theory by Chapman and Enskog model and the turbulent viscosity is calculated according to k-ε model by Launder and Spalding.

### 3.2 HTPB surface pyrolysis model

The pyrolysis of the solid fuel into gaseous products was modeled using the semi-empirical Arrhenius-type relation for regression rate based on the work of Chiaverini et al. and Arisawa and Brill [11]:

$$\dot{r} = A \cdot \exp\left(-\frac{E_a}{R_u T_s}\right) \quad (13)$$

where for surface temperature  $T_s > 722$  K  $E_a = 4.91$  kcal/mole and  $A = 11.04$  mm/s and for  $T_s < 722$  K  $E_a = 13.35$  kcal/mole and  $A = 3965$  mm/s. An additional interfacial energy balance equation on the solid fuel surface was added to determine  $T_s$ . The mass conservation equation is given by:

$$\rho v = -\rho_s \dot{r} \quad (14)$$

As mentioned earlier, Butadiene ( $C_4H_6$ ) is treated as the main product of HTPB pyrolysis and the combustion is described by simplified two-step, one direction chemical reaction:



The eddy dissipation model is selected under the assumption that the combustion process is diffusion controlled i.e., the reaction rate is controlled by the turbulent mixing of the fuel and oxygen.

### 3.3 Boron particle model

Boron particles in the solid fuel are introduced from injections placed on its surface. Under the assumption that volume fraction of boron particles is small compare to gas phase the discrete random walk model is applied to simulate movement of the particles. The particle dynamic equation in Lagrangian reference frame is given by:

$$\frac{d\vec{u}_p}{dt} = \frac{\vec{u} - \vec{u}_p}{\tau_r} + \frac{\vec{g}(\rho_p - \rho)}{\rho_p} + \vec{F} \quad (16)$$

$$\tau_r = \frac{\rho_p d_p^2}{18\mu} \frac{24}{C_D Re} \quad (17)$$

$$Re = \frac{\rho d_p |\vec{u}_p - \vec{u}|}{\mu} \quad (18)$$

The boron particle ignition and combustion is based on King's model. The particle is initially coated with an oxide layer of 0.1-0.2  $\mu\text{m}$  and particle diameter change rate is given by:

$$\frac{d(d_p)}{dt} = -\frac{2R_B M_B}{\pi d_p^2 \rho_B} \quad (19)$$

$$R_B = \frac{0.16 \times 10^{-12} d_p^2 T_p X_{O_2} P}{\delta e^{-22600/T_p}} \quad (20)$$

The oxide thickness  $\delta$  change rate (21) depends on boron reaction rate (20), oxide evaporation rate (22) and reaction rate with water (23):

$$\frac{d(\delta)}{dt} = \frac{(R_B / 2 - R_E - R_H) M_{B_2O_3}}{\pi d_p^2 \rho_{B_2O_3}} \quad (21)$$

$$R_E = \frac{0.32 \times 10^9 \pi d_p^2 (Nu) T_p^{1/2}}{T_p (Nu) + 887 p d_p} e^{-44000/T_p} \quad (22)$$

$$R_H = 4.575 \times 10^{-3} \frac{Nu}{p} d_p T_p^{1/2} e^{18.1(1 - \frac{2100}{T_p})} \cdot [-0.15 + (0.0225 + 0.987 X_{H_2O} p e^{-18.1(1 - \frac{2100}{T_p})})^{1/2}] \quad (23)$$

The particle temperature change rate is given by:

$$\frac{d(T_p)}{dt} = \frac{\dot{Q}_{TOT}}{\frac{\pi}{6} d_p^3 c_{pB} \rho_B + \pi d_p^2 \delta c_{pB_2O_3} \rho_{B_2O_3}} \quad (24)$$

$\dot{Q}_{TOT}$  is the sum of heat rates transferred to particle by convection, radiation, evaporation and chemical reactions. Once the particle reaches melting temperature of 2450 K it starts to melt at rate given by:

$$\frac{df_M}{dt} = -\frac{\dot{Q}_{TOT}}{\frac{\pi}{6} d_p^3 \rho_B \Delta H_M} \quad (25)$$

At this stage the particle temperature remains constant and once it is all melted i.e.  $f_M=1$  the particle temperature change rate is given by:

$$\frac{d(T_p)}{dt} = \frac{\dot{Q}_{TOT}}{\frac{\pi}{6} d_p^3 c_{pBt} \rho_{Bt} + \pi d_p^2 \delta c_{pB_2O_3} \rho_{B_2O_3}} \quad (26)$$

If the oxide layer is completely removed then the particle is ignited, and particle diameter change rate is given by:

$$\frac{d(d_p)}{dt} = -4 \frac{\rho_g D}{\rho_b d_p} \ln(1+B) \quad (27)$$

Where  $B$  is the Spalding number expressed by [1]:

$$B=0.677Y_{O_2} \quad (28)$$

The bypass ratio is defined as the ratio between the main and bypass air:

$$BR = \frac{\dot{m}_b}{\dot{m}_{ai}} \quad (29)$$

### 3.4 Geometry and mesh

Assuming invariance in azimuthal direction the computational domain was reduced to 2-D axisymmetric. A mesh was generated to fit the geometry and grid independence was checked for cold flow simulations so that 86,000 cells mesh was chosen as a compromise between accuracy and computational costs. The mesh was refined toward the wall for proper boundary layer resolution as shown in Fig. 3. The dimensions of the solid fuel and after burner were changed from “without Boron” simulations to “with Boron” simulations.

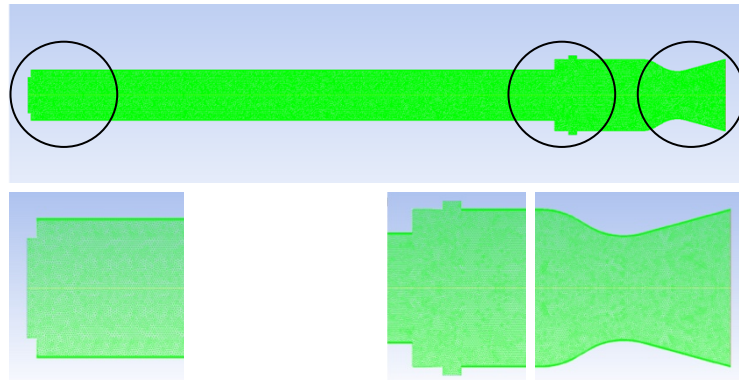


Figure 3: Combustor model mesh.

### 3.5 Numerical solution

Pressure-based coupled solver was used as numerical Algorithm and user defined functions (UDF) were written to describe the above models. Step by step solution was made, starting from cold flow, then reactive flow with UDF describing HTPB model and finally two-phase flow with UDF describing the boron ignition and combustion model. A series of simulations were performed for various parameters such as flight level, solid fuel port diameter, bypass ratio, boron content in solid fuel and boron particle diameter, and the sensitivity of the SFRJ flow field and performance for several parameters were studied. Table 1 shows a summary of simulation parameters.

Table 1: Summary of simulation parameters.

<i>Particle diameter</i> [ $\mu\text{m}$ ]	<i>Boron content</i>	<i>Bypass ratio</i>	<i>Port diameter</i> [mm]	<i>Flight level</i> [ft]
5	5	0.3	70	0
8	10	0.6	75	5000
15	15	0.9	80	10000
20	20	1.2	85	15000
25	25	1.5	90	20000

Remark: light/ dark gray stands for without/ with Boron conditions.

#### 4. Results and Discussion

The simulations were divided into two major parts: simulations without boron that will be used later as a reference point to simulations with boron. Both were compared to NASA CEA thermochemical code results.

##### 4.1 General flow field

Butadiene and oxygen mass fraction, pressure and Mach number flow fields are shown in Fig. 4. The pyrolysis of the solid fuel into gaseous products is noticeable at the top most sub-figures. The average pressure at the combustor is 0.9 MPa and it decreases towards the nozzle outlet. The Mach number is relatively low at the combustor, it reaches Mach 1 at the throat where the flow is choked and average Mach of 2.2 at the nozzle outlet.

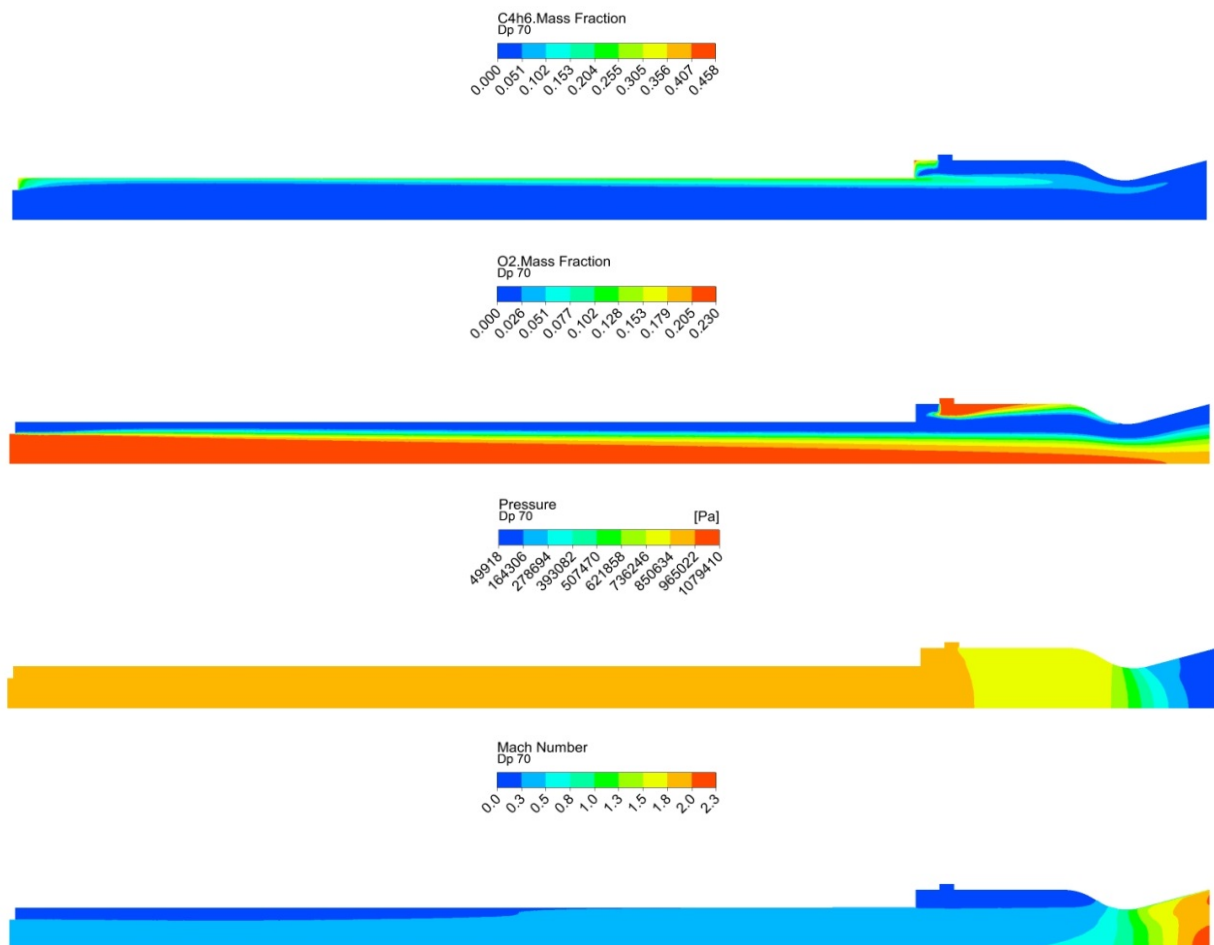


Figure 4: General flow field values.

## 4.2 Port diameter

Solid fuel regression rate for different port diameters is shown in Fig. 5. It is clear that the regression rate is higher at the reattachment zone right after the flame-holding step, it decreases with growing port diameter and thus with time. Similarly to the results of Netzer [11] the recirculation zone length was found to be approximately 6-7 step heights and it moves downstream with growing port diameter.

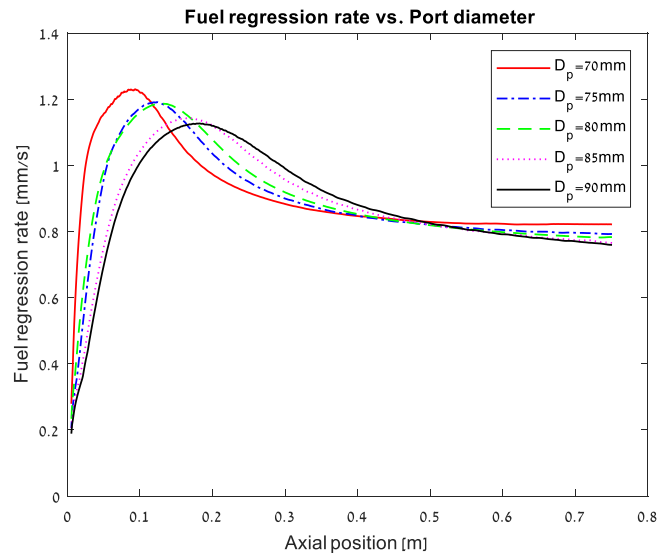


Figure 5: Fuel regression rate vs. axial position for different port diameters.

The temperature flow field for different port diameter is shown in Fig. 6. Port diameter is growing from 70 to 90 mm from the upper to lower figure. It should be noticed that the recirculation zone gets longer and that the reattachment zone moves downstream. As port diameter grows, the flame moves away from the solid fuel surface and the core temperature of the combustor rise.

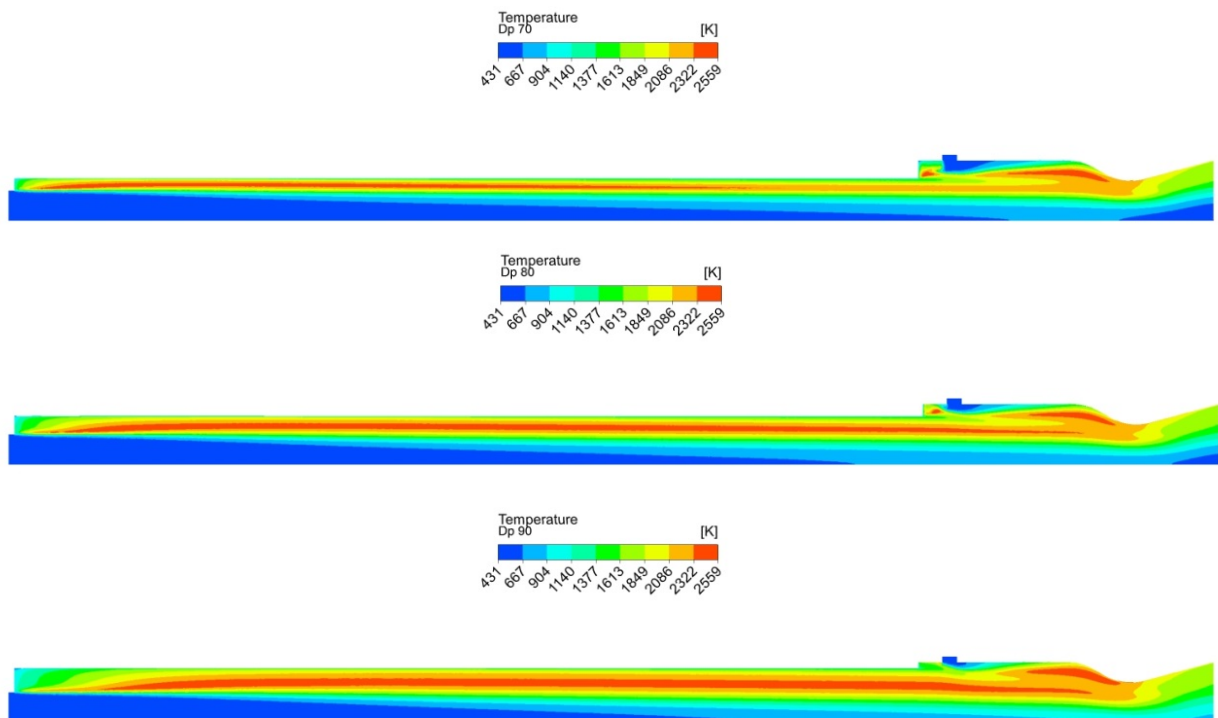


Figure 6: Temperature flow field vs. port diameter.

### 4.3 Bypass ratio

Bypass ratio is the ratio between the main and bypass air, and it has effect on regression rate, fuel flow rate and thrust as shown in figure 7. As bypass ratio increases, i.e. less main air flow, the regression rate decreases as well as the fuel flow rate, equivalent ratio and thrust. This enables, mainly at high bypass ratio ( $BR > 0.5$ ), thrust regulation as was demonstrated in Pelosi and Gany work [12]. At present study bypass ratio of 0.3 was selected for “without Boron” condition and then altered to 0.9 for “with Boron” condition.

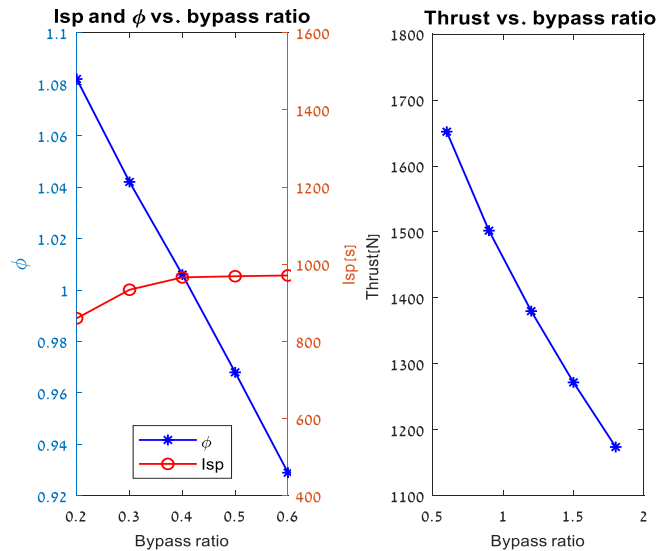


Figure 7: Bypass ratio effect.

### 4.4 Boron particle diameter

Macek has observed that boron particle combustion time depends on the particle initial diameter by  $d^2$  law [8]. In the current work, the relation between particle initial diameter and boron oxide removal time and particle ignition time was studied. Figure 8 shows the relation of boron oxide thickness (which is a key factor in particle ignition process) developing by axial movement and the initial particle diameter changing from 5, 15 and 25  $\mu\text{m}$  top to bottom where the initial boron oxide thickness is 0.1  $\mu\text{m}$ . The parcels of particles are colored by their oxide thickness and one can see that as smaller the initial diameter as shorter the boron oxide removal period.

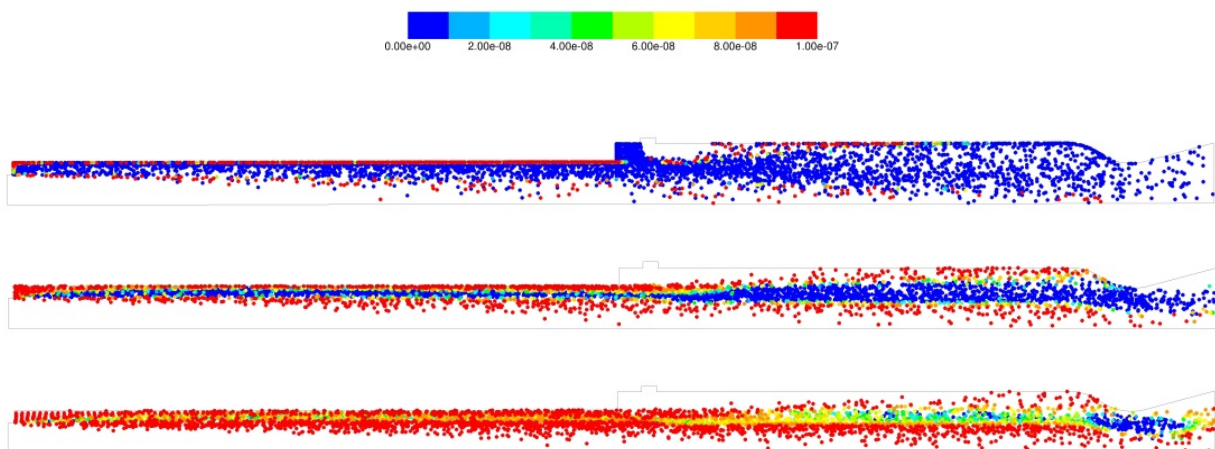


Figure 8: Boron oxide thickness vs. particle initial diameter

As mentioned earlier, boron oxide layer removal is crucial for particle ignition, and Fig. 9 illustrates the relation between the particle temperature and the initial particle diameter. It can be noticed that only 5  $\mu\text{m}$  particles (upper figure) were ignited and the particles temperature is high as 3930 K which is boron boiling temperature.

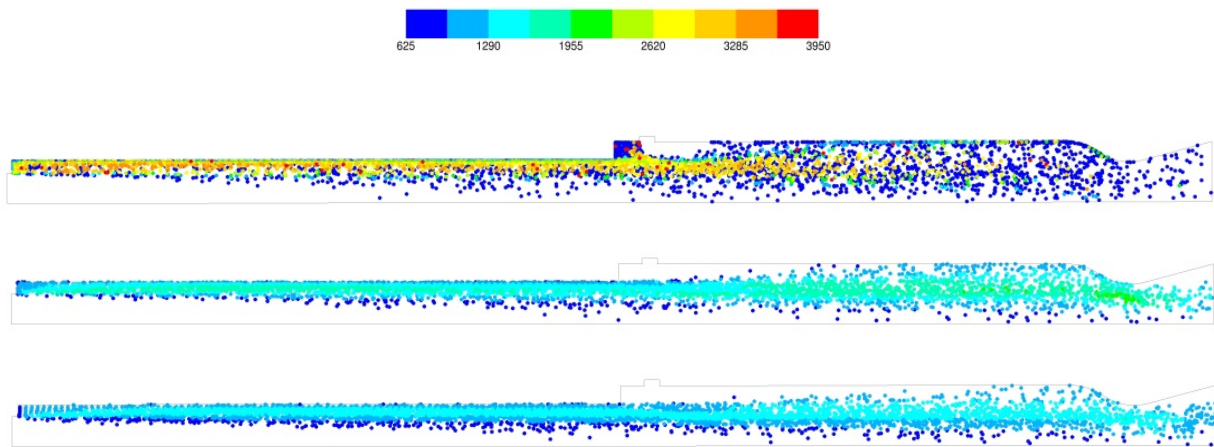


Figure 9: Particle temperature vs. particle initial diameter.

#### 4.5 Boron content

The boron content in the solid fuel (boron mass fraction) has varied from 5% to 25% and the influence on thrust and specific impulse was studied as shown in Fig. 10. It was found that thrust increase with boron content, and on the other hand the specific impulse decrease with boron content. Natan and Gany have found that at low pressure (1 MPa) the specific impulse decreases with boron content because of low combustion efficiency [9] and that it improves at higher pressure (2 MPa).

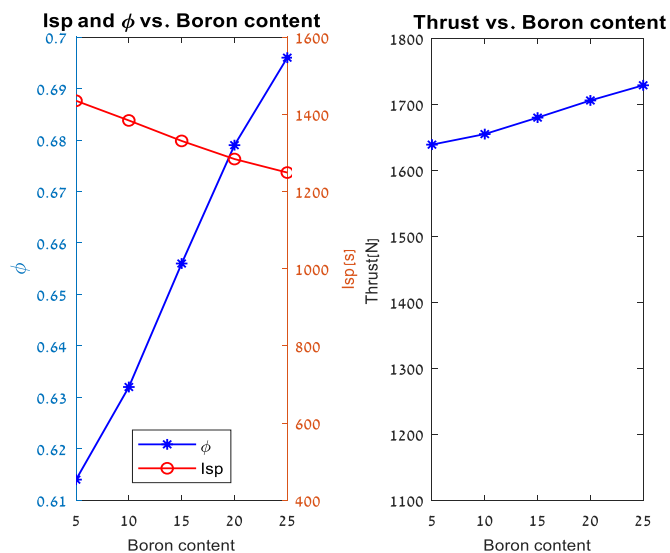


Figure 10: Boron content effect.

A comparison to theoretical results of NASA CEA thermochemical code was made at the same parameters as shown in Fig. 11. It was found that for  $\Phi \approx 0.6$  (5% Boron content) there is a 3.5% difference in Isp. Furthermore, the same phenomenon of decreasing Isp with increasing equivalent ratio for low combustion pressure is evident.

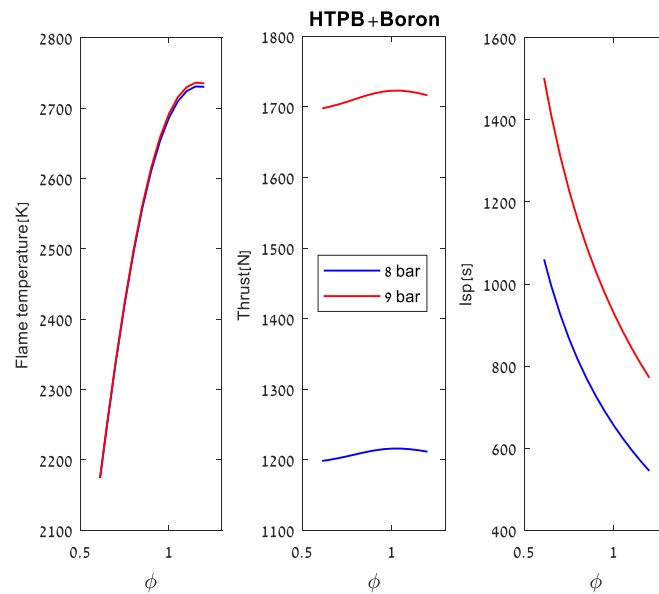


Figure 11: Theoretical performance of HTPB+Boron SFRJ.

## 5. Conclusion

This study focuses on parametric analysis of internal ballistics of a Boron containing SFRJ. A numerical model based on King's model was developed and various simulations were made for different parameters as port diameter, bypass ratio, boron content and particle diameter. Reasonable results comparing to theoretical performance were observed. The solid fuel regression rate depends on the combustor port diameter. It is higher at the reattachment zone right after the flame-holding step and it decreases with growing port diameter and thus with time. Furthermore, the recirculation zone gets larger and the reattachment zone moves downstream with time.

As bypass ratio increases, the regression rate decreases as well and also the fuel flow rate and thrust. Therefore, thrust regulation of ramjet engine is demonstrated using bypass air, mainly at high bypass ratio ( $BR > 0.5$ ).

Boron particle combustion time depends on the particle initial diameter, governed by  $d^2$  law, as well as on boron oxide layer removal. The smaller the boron particle are the faster the boron oxide removal period is and, in our case, only 5  $\mu\text{m}$  particles were ignited at the given combustor dimensions. The specific impulse decreases with boron content probably because of low combustion efficiency at low pressure.

Additional work is desired at higher combustion pressure and longer after burner in order to determine the effect on boron combustion efficiency.

## References

- [1] King, M.K., "Ignition and Combustion of Boron Particles and Clouds," *Journal of Spacecraft*, Vol. 19, No. 4, 1982, pp. 294-306.
- [2] Talley, C.P., "The Combustion of Elemental Boron," *ARS Progress in Astronautics and Rocketry, Solid Propellant Rocket Research*, Vol. 1, 1960, pp. 279-285.
- [3] Gurevich, M.A., Kir'yanov, I.M. and Ozerov, E.S., "Combustion of Individual Boron Particles," *Combustion, Explosion and Shockwaves*, Vol. 5, No. 2, 1969, pp. 150-153.
- [4] Mohan, G. and Williams, F.A., "Ignition and Combustion of Boron in O<sub>2</sub>/Inert Atmospheres," *AIAA Journal*, Vol. 12, 1974, pp. 71-77.
- [5] Glassman, I., Williams, F.A., and Antaki, P., "A Physical and Chemical Interpretation of Boron Particle Combustion," 20th Symposium (International) on Combustion, 1984, pp. 2057-2064.
- [6] Faeth, G.M., "Status of Boron Combustion Research," AFOSR/NA Report, AFOSR Specialists Meeting on Boron Combustion, 1984.
- [7] Yeh, C.L. and Kuo, K.K., "Ignition and Combustion of Boron Particles," *Progress in energy and combustion science*, Vol. 22, No. 6, 1996, pp. 511-541.
- [8] Macek, A. and Semple, J.M., "Combustion of Boron Particles at Atmospheric Pressure," *Combustion Science and Technology*, Vol. 1, 1969, pp. 181-191.

- [9] Natan, B. and Gany, A., "Effect of Bypass Air on the Combustion of Boron Particles in Solid Fuel Ramjets," *Journal of Propulsion and Power*, Vol. 9, No. 1, 1993, pp. 155-157.
- [10] Chiaverini, M.J., Harting, G.C., Lu, Y.C., Kou, K.K., Peretz, A., Jones, H.S., Wygle, B.S. and Arves, J.P., "Pyrolysis Behavior of Hybrid-Rocket Solid Fuels Under Rapid Heating Conditions," *Journal of Propulsion and Power*, Vol. 15, No. 6, 1999, pp. 888-895.
- [11] Netzer, D.W., "Modeling Solid Fuel Ramjet Combustion," *Journal of Spacecraft and Rockets*, Vol. 14, 1977, pp. 762-766.
- [12] Pelosi, D. and Gany, A., "Solid Fuel Ramjet Regulation by Means of an Air Division Valve," *Journal of Propulsion and Power*, Vol. 16, No. 6, 2000, pp. 1069-1074.